Quantum confined Rydberg excitons in reduced dimensions

OPEN ACCESS
IOP Publishing
Journal of Physics B: Atomic, Molecular and Optical Physics
J. Phys. B: At. Mol. Opt. Phys. **53** (2020) 024001 (7pp)
https://doi.org/10.1088/1361-6455/ab56a9

Quantum confined Rydberg excitons in reduced dimensions

Annika Konzelmann, Bettina Frank and Harald Giessen

4th Physics Institute and Research Center SCoPE, University of Stuttgart, D-70569 Stuttgart, Germany

E-mail: h.giessen@pi4.uni-stuttgart.de

Received 7 August 2019, revised 30 September 2019
Accepted for publication 12 November 2019
Published 18 December 2019

Abstract

In this paper we propose first steps towards calculating the energy shifts of confined Rydberg excitons in Cu_2O quantum wells, wires, and dots. The macroscopic size of Rydberg excitons with high quantum numbers n implies that already μm sized lamellar, wire-like, or box-like structures lead to quantum size effects, which depend on the principal Rydberg quantum number n. Such structures can be fabricated using focused ion beam milling of cuprite crystals. Quantum confinement causes an energy shift of the confined object, which is interesting for quantum technology. We find in our calculations that the Rydberg excitons gain a potential energy in the μeV to meV range due to the quantum confinement. This effect is dependent on the Rydberg exciton size and, thus, the principal quantum number n. The calculated energy shifts in the μeV to meV energy range should be experimentally accessible and detectable.

Keywords: Rydberg excitons, cuprous oxide, quantum wells

(Some figures may appear in colour only in the online journal)

1. Introduction

1.1. Rydberg excitons

Rydberg atoms build an important platform for quantum applications because of their long lifetimes and large dipole moments, allowing for the formation of long-range interactions and rendering them highly sensitive for external fields on a quantum level [1–7]. They feature many interesting properties, such as the generation of nonclassical photonic states [8–10], or the dipole blockade [11, 12], which can be used for optical switching and other quantum information processing applications [13–18]. However, their incorporation into the solid state remains difficult.

Rydberg excitons are the solid-state analog of Rydberg atoms. Due to the attractive Coulomb interaction between the conduction electron and the valence hole in a semiconductor, a quasiparticle called exciton can be formed as an excited electronic state of the crystal. This electron–hole pair is weakly bound and extends over many thousands of lattice unit cells, thus its interaction is screened by the static permittivity of the semiconductor (see figure 1(a)). Its energetic levels E_n lie within the semiconductor band gap E_g, while the exciton binding energy $E_b = \mathrm{Ry}^*/(n - \delta_P)^2$ increases with the principal quantum number n as $1/n^2$:

$$E_n = E_g - \mathrm{Ry}^* \frac{1}{(n - \delta_P)^2}. \tag{1}$$

$\mathrm{Ry}^* = \mathrm{Ry}\, m_r/(\varepsilon^2 m_e)$ is the modified Rydberg constant in the semiconductor due to effective electron and hole masses, m_e and m_h, which form a reduced mass $m_r = m_e m_h/(m_e + m_h)$, ε is the background dielectric constant, and δ_P the quantum defect for P-excitons.

This is in analogy to Rydberg atoms, where the outer electron orbits around the nucleus, following the hydrogen formula $E_n = -\mathrm{Ry}/n^2$, with Ry being the Rydberg constant. Now, electron and hole orbit around each other and are termed Rydberg exciton, when being in quantum states with *large* principal quantum number $n \geqslant 10$. The total exciton energy, including its center-of-mass kinetic energy, is

$$E_n = E_g - \mathrm{Ry}^* \frac{1}{(n - \delta_P)^2} + \frac{\hbar^2 K_c^2}{2M}. \tag{2}$$

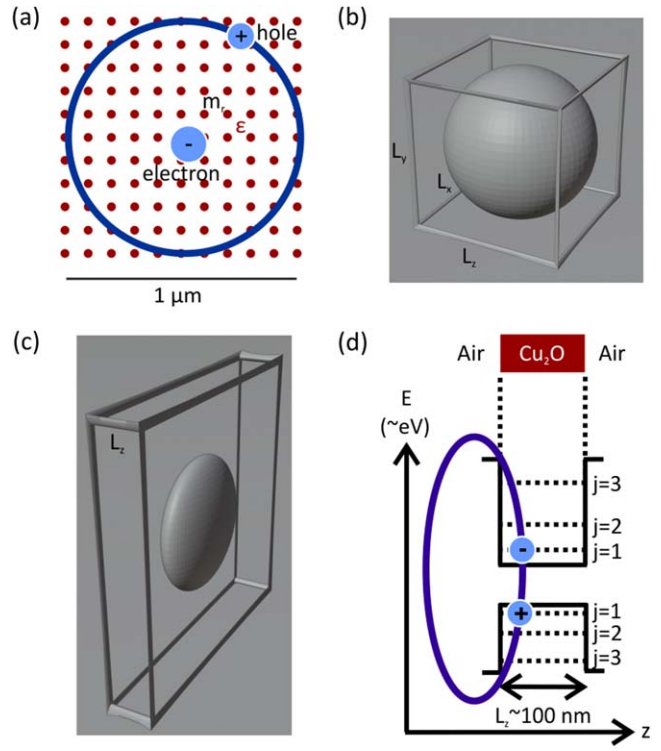

Figure 1. Rydberg excitons in cuprous oxide. (a) With an electron mass $m_e = 0.98 \cdot m_0$ and a hole mass $m_h = 0.68 \cdot m_0$, in cuprous oxide excitons the hole orbits around the electron. Due to the modified masses $m_r = m_e m_h/(m_e + m_h)$ and the crystal environment ε, the cuprite excitons have macroscopic extensions over many thousands of lattice sites and are termed Rydberg excitons in analogy to Rydberg atoms. (b), (c) Rydberg excitons confined in a cuprous oxide box and slab with a width comparable to the exciton diameter. This way the quantum object is weakly confined along the confinement axis. (d) Inside a quantum well, the exciton center-of-mass motion becomes quantized. In the strong confinement regime, electron and hole are even in separate potential wells with energy barriers of a few eV.

The center-of-mass kinetic energy of the exciton usually vanishes for direct band gap semiconductors with band gap energies in the visible due to momentum conservation. Therefore, only a series of sharp lines corresponds to an exciton with vanishing momentum [19]. The crystal ground state is a state with no excited electron–hole pairs; it is totally symmetric with no angular momentum and positive parity.

Cuprous oxide is a semiconductor with outstanding properties [20]. Its band gap $E_g = 2.17$ eV and permittivity $\varepsilon = 9.8$ are particularly large, yielding a very large exciton binding energy $\mathrm{Ry}^* = 96$ meV. This allows for the existence of Rydberg excitons up to principal quantum number $n = 25$ [21]. The exciton Bohr radius for the 1S-exciton is given by:

$$a_B = \frac{h^2 \varepsilon_0 \varepsilon}{\pi m_r e^2}, \tag{3}$$

with h: Planck's constant, ε_0 and ε: vacuum and material permittivity, $m_r = m_e m_h/(m_e + m_h)$: reduced exciton mass with effective electron and hole masses m_e and m_h, and e: electron charge.

These giant Rydberg excitons are very sensitive to external fields due to their huge polarizability (scaling proportional to n^7) [22] and can be easily trapped and positioned in the solid state system [23]. In order to use these giant, highly sensitive quantum objects for quantum technology [1, 2, 24–26], their basic behavior has recently been intensively investigated [27–35].

Excitons are decisive for semiconductor optical properties [36]. The electron–hole relative motion is on a large scale compared to interatomic distances. Therefore, in contrast to Rydberg atoms, which are described by a modified electron wave function only, the exciton wave function Φ^{exc} is given by the electron wavefunction ϕ^e times the hole wavefunction ϕ^h times an envelope wave function ϕ^{env}:

$$\Phi^{exc} = \phi^e \times \phi^h \times \phi^{env}. \tag{4}$$

The envelope wave function describes the electron–hole relative motion, or the angular momentum quantum state l, and can be expressed in spherical harmonics as $Y_0^0 = \sqrt{1/4\pi}$ for S-excitons ($l = 0$) or $Y_1^0 = \sqrt{3/4\pi}\, z/r$ for P-excitons ($l = 1$).

The exciton wave function obeys the two-particle Schrödinger equation (also known as Wannier equation)

$$\left(-\frac{\hbar^2}{2m_e}\nabla_e^2 - \frac{\hbar^2}{2m_h}\nabla_h^2 - \frac{e^2}{\varepsilon_0 \varepsilon |r_e - r_h|}\right)\Phi^{exc} = E\Phi^{exc}, \tag{5}$$

with indices e and h denoting electron and hole, respectively. Equation (4) can be rewritten in relative coordinates only, since the Coulomb term only affects the relative electron–hole coordinates. It then reads:

$$\left(-\frac{\hbar^2}{2m_r}\nabla_r^2 - \frac{e^2}{\varepsilon_0 \varepsilon r}\right)\phi^{env}(\mathbf{r}) = E_r \phi^{env}(\mathbf{r}), \tag{6}$$

with the reduced exciton mass m_r [37].

1.2. Quantum confinement

Rydberg excitons in cuprous oxide quantum wells have not yet been studied, although the concept of the related problem is well known. The problem can be described via potential well calculations. These have already been extensively performed for electrons and holes in semiconductors [38]. Mesoscopic spatial confinements of the order of several μm, also known from quantum dots [39, 40], are still *large* in comparison with the lattice constant of the material. The band structure of a semiconductor is therefore only weakly changed when being spatially confined compared to the bulk material [41]. This assumption allows investigating solely changes in the envelope part of the wave function caused by the confinement potential and is called *envelope function approximation*. However, in spatially confined structures, surface polarization effects may play a role due to the different dielectric constants of the material and its surrounding. This becomes in particular important when investigating Rydberg excitons, which are quasiparticles bound by the three-dimensional Coulomb interaction.

Quantum confinement effects arise as soon as the spatial confinement is comparable to the quantum object's Bohr radius. Rydberg excitons have Bohr radii up to μm size. This allows to confine them in so-called *mesoscopic* structures, the dimension of which is large compared to the lattice constant but comparable to the exciton Bohr radius (see figures 1(b), (c)).

We want to confine a whole Rydberg exciton into a quantum well, and expect large energy shifts of this giant quantum object. In excitons the Coulombic electron–hole attraction gives rise to bound states of the relative motion of the exciton. The excitonic bound levels in quantum wells are, in many respects, analogous to the Coulombic impurity bound states, meaning that the electron and hole relative motion is described by a Hamiltonian which is similar to that of an impurity [42]. We intuitively associate an extra kinetic energy with the localization of a particle in a finite region of space, i.e. the impurity binding energy increases when the quantum well thickness decreases.

1.3. Quantum confined Rydberg excitons

In mesoscopic cuprite slabs surrounded by air or vacuum, the potential barrier accounts for 2.98 eV, which is given by subtracting the Rydberg binding energy (2.17 eV) from the work function energy of electrons in cuprite to air (5.15 eV). This finite potential well energy can, however, be treated as an infinite potential barrier due to the fact that the linear dimension of the confinement exceeds the lattice constant of the semiconductor [41].

In the following, we will focus on the weak confinement regime, where the confinement acts only on the center-of-mass motion of the exciton, i.e. the envelope of the Bloch functions, and does not interfere with the relative motion of the electron–hole pair. Here, the Rydberg exciton binding energies are larger than the confinement effects. In contrast, in the strong confinement limit, the picture of an exciton would be destroyed, as one would then treat electron and hole separately with their individual motions being quantized. In this case, the confinement energy dominates over the Rydberg exciton binding energy.

2. Methods

In order to calculate the energy shifts a Rydberg exciton experiences when being confined in a quantum well, we perform potential well calculations for the center-of-mass coordinate of a Rydberg exciton in a cuprous oxide quantum well (see figure 1(d)). The quantum well consists of a cuprite slab that is extended many micrometers in x and y direction but confined to a few hundreds of nanometers only in z direction. It is surrounded by air or vacuum. Usually, this quantum mechanical problem is not separable due to the confined geometry. In particular, the Coulomb interaction, causing the electron and hole relative motion, is always of three-dimensional nature and depends on the relative electron–hole distance. However, for large quantum wells (weak confinement regime) the confinement or perturbation acts only on the center-of-mass coordinate and is assumed to not disturb the relative motion. Then a separation into relative and center-of-mass coordinates is possible as an approximation.

3. Results

3.1. Electron states for infinite potential barriers

When a quantum object, such as an electron, is spatially confined in one dimension, it gains potential energy $V(z)$, which can be expressed in the Schrödinger equation as:

$$\left[-\frac{\hbar^2}{2m}\nabla^2 + V(z)\right]\psi(x, y, z) = E\psi(x, y, z). \tag{7}$$

The electron wave function can be separated into $\psi(x, y, z) = \phi(x, y)\,\varsigma(z)$, which allows for solving the Schrödinger equation via the separation ansatz:

$$-\frac{\hbar^2}{2m}\nabla_\perp^2\phi(x, y) = E_\perp\phi(x, y) \tag{8}$$

and

$$\left[-\frac{\hbar^2}{2m}\frac{\partial^2}{\partial z^2} + V(z)\right]\varsigma(z) = E_z\varsigma(z). \tag{9}$$

Equation (8) yields the particle kinetic energy $E_\perp = \frac{\hbar^2}{2m}(k_x^2 + k_y^2)$, which is comparable to equation (2) for the exciton, while equation (9) determines the particle's quantized energy eigenvalues due to the quantum confinement

$$E_z = \frac{\hbar^2\pi^2}{2m}\left(\frac{j}{L_z}\right)^2, \tag{10}$$

with j being the quantum state index in the quantum well and L_z the well width. The quantized bound state energies increase with decreasing quantum well width and are proportional to the quantum state index j^2.

3.2. Weakly confined Rydberg excitons in cuprite quantum wells

Following the calculation scheme from the previous section, we calculate the Rydberg exciton energies in a cuprite quantum well with quasi-infinite potential well barrier

$$V_0(z_{e,h}) = \begin{cases} 2.98\ \text{eV}, & |z_{e,h}| > L_z/2 \\ 0\ \text{eV}, & |z_{e,h}| < L_z/2 \end{cases}. \tag{11}$$

The Hamiltonian describing this problem is given by

$$\begin{aligned} H &= -\frac{\hbar^2}{2m_e}\nabla_e^2 - \frac{\hbar^2}{2m_h}\nabla_h^2 + V_{Confinement} + V_{Coulomb} \\ &= -\frac{\hbar^2}{2m_e}\left(\frac{\partial^2}{\partial x_e^2} + \frac{\partial^2}{\partial y_e^2} + \frac{\partial^2}{\partial z_e^2}\right) \\ &\quad - \frac{\hbar^2}{2m_h}\left(\frac{\partial^2}{\partial x_h^2} + \frac{\partial^2}{\partial y_h^2} + \frac{\partial^2}{\partial z_h^2}\right) \\ &\quad + V_0(z_{e,h}) - \frac{e^2}{\epsilon_0|r_e - r_h|}, \end{aligned} \tag{12}$$

and reads in relative and center-of-mass coordinates:

$$H = -\frac{\hbar^2}{2m_e}\frac{\partial^2}{\partial z_e^2} - \frac{\hbar^2}{2m_h}\frac{\partial^2}{\partial z_h^2} - \frac{\hbar^2}{2M_{xy}}\left(\frac{\partial^2}{\partial X^2} + \frac{\partial^2}{\partial Y^2}\right) - \frac{\hbar^2}{2m_{xy}}\left(\frac{\partial^2}{\partial x^2} + \frac{\partial^2}{\partial y^2}\right) + V_0(z_{e,h}) - \frac{e^2}{\epsilon_0 r}, \tag{13}$$

Applied to the exciton wave function this yield a series of bound exciton lines at energy positions:

$$E_n^{2D} = E_g - \mathrm{Ry}^*\frac{1}{(n-\delta_P)^2} + \frac{\hbar^2\pi^2}{2m_r}\left(\frac{j}{L_z}\right)^2. \tag{14}$$

This is similar to equation (1) but with an additional quantized energy term $\Delta_{conf} = \hbar^2\pi^2 j^2/(2m_r L_z^2)$ due to quantum confinement in one dimension, with j being the quantum state index and L_z being the quantum well width.

3.2.1. Rydberg exciton diameters versus quantum well sizes. From quantum dots it is known that for confinements smaller than $0.4 \cdot a_B$, excitons break up [41]. On the other hand, for well widths $L_z \approx 4 \cdot a_B$, the energy shift should be most pronounced. Furthermore, we investigate weakly confined Rydberg excitons, i.e. Rydberg excitons in quantum wells of sizes $L_z \geqslant 4 \cdot r$. As the Rydberg exciton radius increases with increasing principal quantum number n, we define $\Delta_L = L_z - 2r$, as the confinement parameter of interest. This allows to include the n dependence of the confinement potential for a certain confinement length L_z. We calculated the Rydberg P-exciton radii in cuprite according to $r = 0.5 * a_B^{Cu_2O}(3n^2 - l(l+1))$, with n and l being the principal and angular momentum quantum number, respectively, and $a_B^{Cu_2O} = a_B^H \varepsilon m_e/m_r$, with a_B^H: Bohr radius, m_e: electron mass, m_r: reduced mass of exciton in Cu_2O, ε: Cu_2O permittivity. The confinement parameter Δ_L for four different confinement lengths L_z is plotted in figure 2 together with the exciton diameter $d = 2r$ for excitons in different principal quantum number states $n = 2 \ldots 20$. The weak confinement regime holds in 2 μm wide quantum wells for Rydberg excitons in principal quantum number states up to $n = 16$, in 1.5 μm wide wells up to $n = 13$, in 1 μm wide wells up to $n = 11$, and in 500 nm wide wells up to $n = 8$. The higher the principal quantum number state, the larger the exciton, the smaller the remaining space in the quantum well and, thus, the smaller the confinement parameter Δ_L.

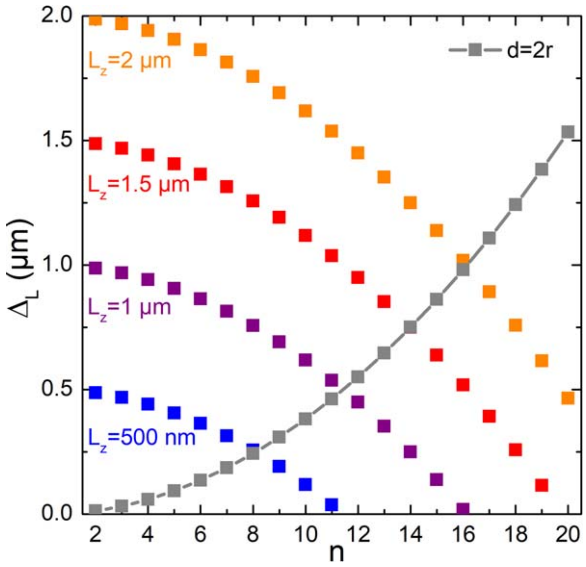

Figure 2. Confinement parameter $\Delta_L = L_z - 2r$ and P-exciton diameter $d = 2r$ for four different confinement lengths L_z in dependence of the principal quantum number $n = 2 \ldots 20$.

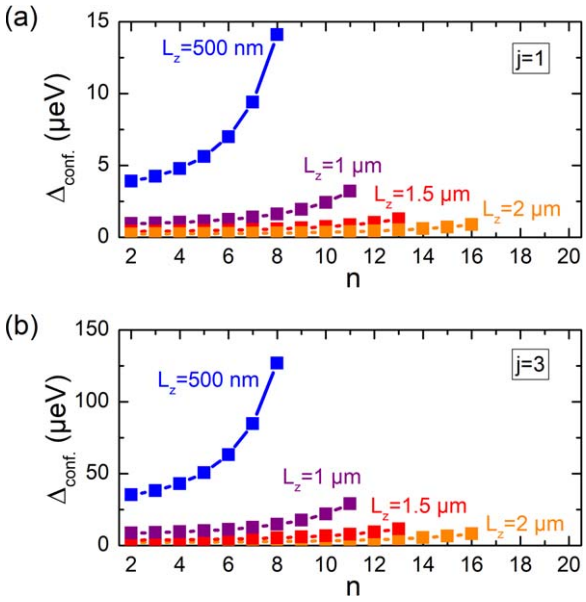

Figure 3. (a) Energy gain Δ_{conf} due to the quantum confinement for the lowest quantum state index $j = 1$ for four different well widths $L_z \in \{0.5,\ 1,\ 1.5,\ 2\}$ μm in dependence on the principal quantum number n. The lines are guides to the eye. (b) Same data but for the quantum state index $j = 3$.

3.2.2. Rydberg exciton energy shift. Quantum confinement along one dimension causes an increase in potential energy of the confined Rydberg exciton dependent on the confinement parameter Δ_L, the confinement quantum state j and the quantum object mass m_r. We show in figure 3 the calculated energy blue-shifts $\Delta_{conf} = \hbar^2\pi^2 j^2/(2m_r\Delta_L^2)$ experienced by Rydberg excitons in cuprite quantum wells for the lowest and third excited quantum state $j = 1$ and $j = 3$, respectively, and for four different well widths $L_z \in \{0.5; 1; 1.5; 2\}$ μm. The data are only shown within in the weak confinement regime, which applies for Rydberg excitons with up to a different amount of principal quantum number n for different quantum well sizes L_z (see also figure 2).

For both, the lowest ($j = 1$) and third excited ($j = 3$) quantum state index, and for all different well widths L_z shown here, the energy shift Δ_{conf} increases with increasing principal quantum number n. This increase in energy is absolutely larger and steeper the smaller the well widths. For the lowest quantum state index $j = 1$, Δ_{conf} accounts for up to 14 μeV, while for the third excited quantum state index

$j = 3$ Δ_{conf} reaches values of up to 140 μeV, which is one order of magnitude larger.

3.3. Strongly confined Rydberg excitons in cuprite quantum wells

Subject of this paper is the weak quantum confinement of Rydberg excitons in cuprite quantum wells. The relevant structures are of several hundreds of nanometers to a few micrometers in size, which can be procuded straight-forwardly using focused ion beams. Furthermore, we want to investigate a single, giant quantum object—the Rydberg exciton. In the strong confinement regime, the confinement energy would exceed the Coulomb energy and thus the binding energy of the exciton. In this case, electron and hole are confined separately in their respective confinement potentials. We believe that the following considerations regarding the strong confinement regime might be of interest for the reader.

3.3.1. Exciton binding energy in the strict 2D limit. The 3D Rydberg P-exciton energy is given by $E_n = E_g - E_b = E_g - \mathrm{Ry}^*/(n - \delta_P)^2$, with E_g: band gap energy, Ry^*: Rydberg constant for excitons in cuprous oxide, n: principal quantum number, and $\delta_P = 0.23$: quantum defect for P-excitons [43]. In *strictly* two dimensions, the Rydberg exciton binding energy E_b becomes modified into $E_b^{2D} = \mathrm{Ry}^*/(n - 1/2)^2$ [44]. This implies that the lowest 2D exciton energy ($n = 1$) has a magnitude four times larger than the 3D exciton ground state, when neglecting the quantum defect: $E_{b,n=1}^{2D} = 4E_b$. Thus, the exciton ground state is farther away from the bandgap in 2D and the 2D Bohr radius $a_B^{2D} = a_B^{3D}/2$ is half as big as the 3D value. The excitonic resonances as well as the exciton binding energies are stronger in 2D. Interestingly, the absorption strength decreases in this situation more rapidly with n. The transition from 3D to 2D would cause exciton energy shifts of even a few meV:

$$\Delta^{2D} = E_n - E_n^{2D} = E_g - E_b - (E_g - E_b^{2D}) = -E_b + E_b^{2D} = -\frac{\mathrm{Ry}^*}{(n - \delta_P)^2} + \frac{\mathrm{Ry}^*}{(n - 1/2)^2}. \quad (15)$$

The exciton binding energy in three dimensions decreases rapidly with n. So does the binding energy in two dimensions as well, however, at some larger values. The difference of both, defined as the energy shift Δ^{2D}, thus, follows the same trend. Note that a larger Rydberg binding energy implies a smaller Rydberg exciton energy as the binding energy (~meV) is subtracted from the band gap energy (~eV) in order to yield the exciton energy $E_n = E_g - E_b$. Therefore, the effect the 2D confinement will have on the total exciton energy will be a red-shift toward lower energies.

3.3.2. Influence of the permittivity of the surrounding material outside the quantum well. In the case of a very narrow quantum well, the permittivity inside and outside the well is different. The Coulomb interaction between electron and hole in an exciton is of three-dimensional character and, thus, not squeezed inside the well, but occurs primarily outside the well with less effective screening [45]. The binding energy would then become:

$$E_b^{2D*} = \left(\frac{2\varepsilon}{\varepsilon_\mathrm{I} + \varepsilon_\mathrm{III}}\right)^2 \frac{\mathrm{Ry}^*}{(n - 1/2)^2}, \quad (16)$$

with $\varepsilon = 9.8$: cuprous oxide permittivity and $\varepsilon_\mathrm{I} = \varepsilon_\mathrm{III} = 1$: air permittivity surrounding the narrow well structure. This would imply another increase in binding energy of almost two orders of magnitude:

$$\left(\frac{2\varepsilon}{\varepsilon_\mathrm{I} + \varepsilon_\mathrm{III}}\right)^2 = \left(\frac{2 * 9.8}{2}\right)^2 = (9.8)^2 = 96.04 \approx 10^2.$$

4. Discussion

The quantum confinement inhibits free motion and, thus, influences the kinetic energy of the quantum object. Only discrete values are allowed, leading to a series of quantized states [46]. Confined to a quantum well, Rydberg excitons gain energy, so they experience an energy blue-shift. Within the weak confinement regime, this energy shift accounts for a few and a few tens of μeV for the lowest and third excited quantum state index, respectively.

The energy shifts are controllable via the three parameters principal quantum number n, quantum state index in the quantum well j, and quantum well width L_z over a wide range. Such controllable energy shift could be used for realizing quantum technologies using Rydberg excitons in cuprous oxide [2]. In order to enlarge the range over which the energy can be shifted, one could go to higher confinements, meaning a more tight confinement along one dimension (intermediate or strong confinement regime in 2D).

The conditions for the strong confinement regime become, as shortly discussed in section 3.3, more complicated. Strictly speaking, for a very strong exciton confinement, electron and hole become quantized separately, so the quantization energy dominates over the Coulomb interaction energy and we cannot speak of an exciton any more. In order to get a feeling for how the energy shifts would develop when going towards the intermediate regime ($L_z \approx 2r$), we applied our weak confinement model to excitons in this intermediate confinement regime. The resulting energy blue-shifts Δ_{conf} are depicted in figure 4 for the lowest quantum state index $j = 1$, for different well widths L_z, and in dependence on the principal quantum number n.

The transition from the weak to the intermediate regime is smooth. As expected, the energy blue-shifts become significantly larger the narrower the quantum wells, and account for up to several tens of meV. In the strong confinement regime, the electron and hole confinement energies would exceed the exciton binding energy $\mathrm{Ry}^* = 96$ meV.

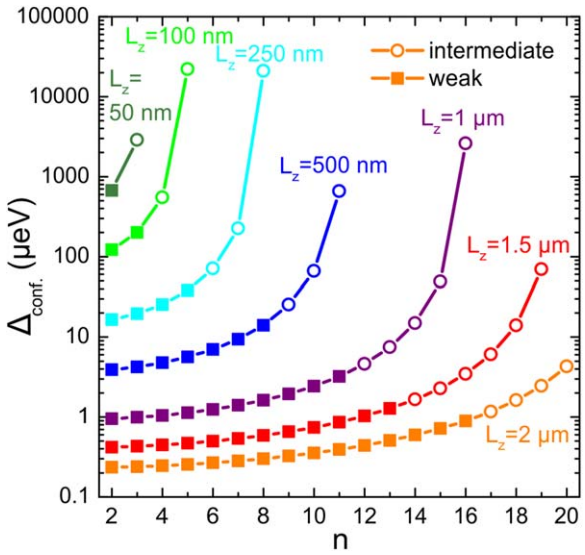

Figure 4. Energy shifts in μeV due to quantum confinement Δ_{conf} for the lowest quantum state index $j = 1$, for weak ($L_z \geqslant 4r$, squares) and intermediate ($2r < L_z < 4r$, circles) regimes. The energy shifts are shown in dependence on the principal quantum number n and for seven different well widths L_z. The strong confinement regime begins where $\Delta_{conf} \approx E_b = 96$ meV; this is at the top of the diagram.

5. Outlook

Higher quantum confinements can also be reached by confining a quantum object in two or three dimensions. This can be realized by confining Rydberg excitons into cuprite quantum wires or quantum dots (see figure 1(b)). In such structures the energy shift caused by the confinement geometry reads:

$$\Delta_{conf}^{1D} = \frac{\hbar^2\pi^2}{2m_r}\left(\frac{j_z^2}{L_z^2} + \frac{j_y^2}{L_y^2}\right) \xrightarrow{L_z=L_y} 2 \cdot \Delta_{conf}^{2D} \qquad (17)$$

and

$$\Delta_{conf}^{0D} = \frac{\hbar^2\pi^2}{2m_r}\left(\frac{j_z^2}{L_z^2} + \frac{j_y^2}{L_y^2} + \frac{j_x^2}{L_x^2}\right) \xrightarrow{L_z=L_y=L_x} 3 \cdot \Delta_{conf}^{2D}. \qquad (18)$$

The blue-shift could, thus, be enhanced by a factor of 2 and 3 compared to the quantum well structures. It remains, however, unknown how the Rydberg binding energy would change in such structures.

Recent advances in focused ion beam milling using Au^+ ions (Raith IonLine) make it possible to fabricate tailored quantum wells with widths in the hundreds of nm range, as shown in figure 5. Therefore one should in principle be able to weakly confine experimentally Rydberg excitons into quantum wells. The difficulty remains in that the well interface needs to be very flat, to not disturb the crystal lattice, its symmetry, and thus the exciton formation. The energy shifts could be measured in absorption or by pump-probe spectroscopy. This gives for the first time the opportunity to probe such large quantum objects inside the confined geometry of quantum wells.

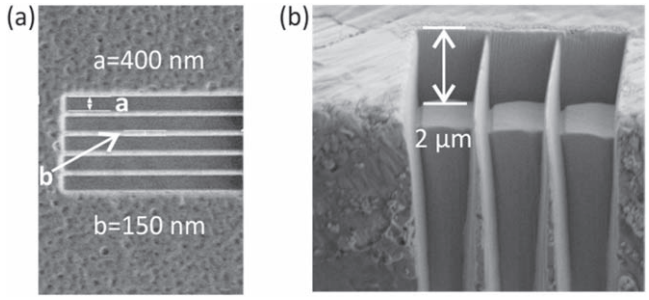

Figure 5. Cuprous oxide quantum wells for Rydberg excitons. The huge size of the Rydberg excitons allows mesoscopic confinement geometries in the hundreds of nanometer to a few micrometer range that can be fabricated using focused ion beams.

Acknowledgments

We gratefully acknowledge funding by the Deutsche Forschungsgemeinschaft (DFG, SPP1929) and the European Research Council (ERC, Complexplas).We thank S W Koch and G Quinteiro for fruitful discussions and T Pohl and F Sterl for graphical rendering.

ORCID iDs

Annika Konzelmann https://orcid.org/0000-0002-8263-1353
Bettina Frank https://orcid.org/0000-0002-7602-5154
Harald Giessen https://orcid.org/0000-0002-4270-3850

References

[1] Gallagher T F 1988 Rydberg atoms *Rep. Prog. Phys.* **51** 143–88
[2] Saffman M, Walker T G and Molmer K 2010 Quantum information with Rydberg atoms *Rev. Mod. Phys.* **82** 2313–63
[3] Schauß P, Cheneau M, Endres M, Fukuhara T, Hild S, Omran A, Pohl T, Gross C, Kuhr S and Bloch I 2012 Observation of spatially ordered structures in a two-dimensional Rydberg gas *Nature* **491** 87–91
[4] Labuhn H, Barredo D, Ravets S, De Léséleuc S, Macrì T, Lahaye T and Browaeys A 2016 Tunable two-dimensional arrays of single Rydberg atoms for realizing quantum Ising models *Nature* **534** 667–70
[5] Bernien H *et al* 2017 Probing many-body dynamics on a 51-atom quantum simulator *Nat. Publ. Gr.* **551** 579–84
[6] Gleyzes S, Kuhr S, Guerlin C, Bernu J, Deléglise S, Busk Hoff U, Brune M, Raimond J M and Haroche S 2007 Quantum jumps of light recording the birth and death of a photon in a cavity *Nature* **446** 297–300
[7] Crowley T P, Donley E A and Heavner T P 2004 Quantum-based microwave power measurements: Proof-of-concept experiment *Rev. Sci. Instrum.* **75** 2575–80
[8] Peyronel T, Firstenberg O, Liang Q, Hofferberth S, Gorshkov A V, Pohl T, Lukin M D and Vuletic V 2012

Quantum nonlinear optics with single photons enabled by strongly interacting atoms *Nature* **57** 8–11
[9] Firstenberg O, Peyronel T, Liang Q Y, Gorshkov A V, Lukin M D and Vuletić V 2013 Attractive photons in a quantum nonlinear medium *Nature* **502** 71–5
[10] Ripka F, Kübler H, Löw R and Pfau T 2018 A room-temperature single-photon source based on strongly interacting Rydberg atoms *Science* **362** 446–9
[11] Lukin M D, Fleischhauer M and Cote R 2001 Dipole blockade and quantum information processing in mesoscopic atomic ensembles *Phys. Rev. Lett.* **87** 1–4
[12] Comparat D and Pillet P 2010 Dipole blockade in a cold Rydberg atomic sample [Invited] *J. Opt. Soc. Am.* B **27** A208
[13] Isenhower L, Urban E, Zhang X L, Gill A T, Henage T, Johnson T A, Walker T G and Saffman M 2010 Demonstration of a neutral atom controlled-NOT quantum gate *Phys. Rev. Lett.* **104** 8–11
[14] Jau Y Y, Hankin A M, Keating T, Deutsch I H and Biedermann G W 2016 Entangling atomic spins with a Rydberg-dressed spin-flip blockade *Nat. Phys.* **12** 71–4
[15] Tiarks D, Schmidt S, Rempe G and Dürr S 2016 Optical π phase shift created with a single-photon pulse *Sci. Adv.* **2** 1–6
[16] Baur S, Tiarks D, Rempe G and Dürr S 2014 Single-photon switch based on Rydberg blockade *Phys. Rev. Lett.* **112** 1–5
[17] Tiarks D, Baur S, Schneider K, Dürr S and Rempe G 2014 Single-photon transistor using a Förster resonance *Phys. Rev. Lett.* **113** 1–5
[18] Gorniaczyk H, Tresp C, Schmidt J, Fedder H and Hofferberth S 2014 Single-photon transistor mediated by interstate Rydberg interactions *Phys. Rev. Lett.* **113** 1–5
[19] Daunois A and Deiss J 1973 Modulated exciton spectroscopy *Surf. Sci.* **37** 804–27
[20] Gross E F 1956 Optical spectrum of excitons in the crystal lattice *Suppl. Nuovo Cimento* **4** 672–701
[21] Kazimierczuk T, Fröhlich D, Scheel S, Stolz H and Bayer M 2014 Giant Rydberg excitons in the copper oxide Cu_2O *Nature* **514** 343–7
[22] Heckötter J, Freitag M, Fröhlich D, Aßmann M, Bayer M, Semina M A and Glazov M M 2017 Scaling laws of Rydberg excitons *Phys. Rev. B* **96** (12) 125142
[23] Krüger S O and Scheel S 2018 Waveguides for Rydberg excitons in Cu_2O from strain traps *Phys. Rev.* B **97** 1–8
[24] Sedlacek J A, Schwettmann A, Kübler H, Löw R, Pfau T and Shaffer J P 2012 Microwave electrometry with Rydberg atoms in a vapour cell using bright atomic resonances *Nat. Phys.* **8** 819–24
[25] Bendkowsky V, Butscher B, Nipper J, Shaffer J P, Löw R and Pfau T 2009 Observation of ultralong-range Rydberg molecules *Nature* **458** 1005–8
[26] Heidemann R, Raitzsch U, Bendkowsky V, Butscher B, Löw R, Santos L and Pfau T 2007 Evidence for coherent collective Rydberg excitation in the strong blockade regime *Phys. Rev. Lett.* **99** 163601
[27] Walther V, Krüger S O, Scheel S and Pohl T 2018 Interactions between Rydberg excitons in Cu_2O *Phys. Rev.* B **98** 1–6
[28] Konzelmann A M, Krüger S O and Giessen H 2019 Interaction of OAM light with Rydberg excitons: modifying dipole selection rules *Phys. Rev.* B **100** 115308
[29] Kitamura T, Takahata M and Naka N 2017 Quantum number dependence of the photoluminescence broadening of excitonic Rydberg states in cuprous oxide *J. Lumin.* **192** 808–13
[30] Heckötter J, Freitag M, Aßmann M, Fröhlich D and Bayer M 2018 Critical dependence of the excitonic absorption in cuprous oxide on experimental parameters *Phys. Solid State* **60** 1618–24
[31] Schweiner F, Main J, Wunner G and Uihlein C 2017 Even exciton series in Cu_2O *Phys. Rev.* B **95** 195201
[32] Quinteiro G F 2010 Below-bandgap excitation of bulk semiconductors by twisted light *Europhys. Lett.* **91** 27002
[33] Kuhn T, Reiter D E and Quinteiro G F 2015 Optical control of exciton and spin states in a quantum dot by excitation with twisted light *J. Phys.: Conf. Ser.* **647** 012012
[34] Quinteiro G F and Tamborenea P I 2009 Theory of the optical absorption of light carrying orbital angular momentum by semiconductors *Europhys. Lett.* **85** 47001
[35] Zielińska-Raczyńska S, Czajkowski G and Ziemkiewicz D 2016 Optical properties of Rydberg excitons and polaritons *Phys. Rev.* B **93** 1–11
[36] Klingshirn C F 2012 *Semiconductor Optics* (Berlin: Springer)
[37] Peyghambarian N, Koch S W and Mysyrowicz A 1993 *Introduction to Semiconductor Optics* (Englewood Cliffs, NJ: Prentice-Hall)
[38] Bastard G, Mendez E E, Chang L L and Esaki L 1982 Exciton binding energy in quantum wells *Phys. Rev.* B **26** 1974–9
[39] Thoai D B T, Hu Y Z and Koch S W 1990 Influence of the confinement potential on the electron–hole-pair states in semiconductor microcrystallites *Phys. Rev.* B **42** 11261–6
[40] Einevoll G T 1992 Confinement of excitons in quantum dots *Phys. Rev.* B **45** 3410–7
[41] Bányai L and Koch S W 1993 *Semiconductor Quantum Dots* (Singapore: World Scientific)
[42] Bastard G 1988 *Wave Mechanics Applied to Semiconductor Heterostructures* (New York: Halsted Press)
[43] Schöne F, Krüger S O, Grünwald P, Aßmann M, Heckötter J, Thewes J, Stolz H, Fröhlich D, Bayer M and Scheel S 2016 Coupled valence band dispersions and the quantum defect of excitons in Cu_2O *J. Phys. B: At. Mol. Opt. Phys.* **49** 134003
[44] Chernikov A, Berkelbach T C, Hill H M, Rigosi A, Li Y, Aslan O B, Reichman D R, Hybertsen M S and Heinz T F 2010 Exciton binding energy and nonhydrogenic Rydberg series in monolayer WS_2 *Phys. Rev. Lett.* **113** 076802
[45] Grönqvist J H, Stroucken T, Berghäuser G and Koch S W 2011 Excitons in graphene and the influence of the dielectric environment (arXiv:1107.5653v1)
[46] Haug H and Koch S W 1993 *Quantum Theory of the Optical and Electronic Properties of Semiconductors* (Singapore: World Scientific)